Analysis of intermittency in under-resolved smoothed-particle-hydrodynamics direct numerical simulations of forced compressible turbulence

Yilei Shi,* Marco Ellero, and Nikolaus A. Adams

Lehrstuhl für Aerodynamik und Strömungsmechanik, Technische Universität München, Boltzmannstr. 15, 85748 Garching, Germany

(Received 3 November 2011; published 22 March 2012)

We perform three-dimensional under-resolved direct numerical simulations of forced compressible turbulence using the smoothed particle hydrodynamics (SPH) method and investigate the Lagrangian intermittency of the resulting hydrodynamic fields. The analysis presented here is motivated by the presence of typical stretched tails in the probability density function (PDF) of the particle accelerations previously observed in two-dimensional SPH simulations of uniform shear flow [Ellero *et al.*, Phys. Rev. E **82**, 046702 (2010)]. In order to produce a stationary isotropic compressible turbulent state, the real-space stochastic forcing method proposed by Kida and Orszag is applied, and the statistics of particle quantities are evaluated. We validate our scheme by checking the behavior of the energy spectrum in the supersonic case where the expected Burgers-like scaling is obtained. By discretizing the continuum equations along fluid particle trajectories, the SPH method allows us to extract Lagrangian statistics in a straightforward fashion without the need for extra tracer particles. In particular, Lagrangian PDF of the density, particle accelerations as well as their Lagrangian structure functions and local scaling exponents are analyzed. The results for low-order statistics of Lagrangian intermittency in compressible turbulence demonstrate the implicit subparticle-scale modeling of the SPH discretization scheme.

DOI: 10.1103/PhysRevE.85.036708 PACS number(s): 47.11.−j, 47.27.−i, 47.40.−x

I. INTRODUCTION

The numerical investigation of the statistical properties of turbulence from the Lagrangian point of view is becoming increasingly accessible due to the recent improvement of experimental equipment [1] and computational capabilities for direct numerical simulation (DNS) [2]. The Lagrangian properties of turbulence are important for understanding turbulent diffusion and turbulent mixing. Although experimental techniques have improved considerably in the last few years, there are still several limitations, such as particle size [3,4], spatial resolution [5], and maximal number of tracked particles [6].

Numerical simulations allow to access multitime, multiparticle correlations statistics in a straightforward manner. From the computational point of view a major limitation of DNS is the rapid increase in computational cost with increasing Reynolds number, so that in practice only moderate Reynolds numbers can be reached. Another issue is the need for generating sufficient independent statistical samples for analysis. Lagrangian simulations for very high resolutions currently cover only a few large-eddy turnover times. Advantages and limitations of particle tracking based on Eulerian DNS have been recently reviewed by Toschi and Bodenschatz [7].

In recent years many methods have been developed to simulate fluid flow in a Lagrangian framework. Among them the smoothed particle hydrodynamics (SPH) is a popular meshfree, Lagrangian particle method which has been originally designed to address astrophysical flow problems on three-dimensional unbounded domains [8,9]. Later it has been applied for the modeling of fluids in a wide range of complex situations [10]. For the simulation of turbulence, Price [11] compared the statistics of driven, supersonic turbulence at high Mach number using the piecewise parabolic method (PPM) Eulerian grid-based code and a Lagrangian SPH code at resolutions of up to 512^3 in both grid cells and SPH particles. Excellent agreement was found between the two methods on the basic statistical properties, such as the probability density function (PDF) of the density, and the power spectrum. This implies that Lagrangian DNS using SPH can be a feasible alternative to grid-based methods.

Although having the noticeable advantage to operate directly in a Lagrangian framework, high-resolution DNS using SPH are nevertheless very time consuming, and this computational bottleneck does not usually allow for fully resolved simulations at desirable Reynolds numbers even on the largest particle resolution considered, $N = 512^3$ [11]. However, it might be not necessary to have fully resolved results when studying qualitatively the basic phenomena of intermittency, where reasonable accurate estimates of low-order statistics could be sufficient. This is the motivation for the present paper, namely, to explore whether low-resolution SPH simulations are a suitable tool for such a purpose.

An analysis of Lagrangian intermittency in three-dimensional forced compressible turbulence is performed intentionally using under-resolved SPH simulations. The analysis presented here is motivated by the presence of typical stretched tails (namely, high probability of large acceleration events compared to a Gaussian distribution) in the PDF of particle accelerations previously observed in two-dimensional simulations under constant shear flow [12] which qualitatively resemble those obtained for Lagrangian tracers in fully developed incompressible turbulence [7]. In order to produce a steady isotropic compressible turbulent state, the stochastic forcing scheme proposed by Kida *et al.* [13] and the statistics of particle quantities are analyzed. In particular, energy spectra, PDF of the density and particle accelerations, as well as their Lagrangian structure functions are analyzed, and the impact of Reynolds and Mach numbers on the observed intermittent behavior is discussed.

*yilei.shi@aer.mw.tum.de

The paper is organized as follows. In Sec. II the basic SPH formulations used in this work are reviewed. In Sec. III the forcing scheme used in our simulation is discussed. Results of our simulations in the case of forced isotropic compressible turbulence are presented in Sec. IV, where the energy spectrum, PDF of density, PDF of acceleration, and scaling exponents are studied in detail. Finally, conclusions are given in Sec. V.

II. SPH METHOD

Smoothed particle hydrodynamics (SPH) is a fully Lagrangian technique for modeling fluids where the numerical solution is obtained by interpolation on an arbitrary set of points instead of a fixed grid. The basic ingredient of SPH is represented by an interpolation process which allows any function A to be expressed in terms of its values defined on a set of disordered points (particles) [8,9]. The integral interpolations of $A(\mathbf{r})$ reads therefore

$$A(\mathbf{r}) = \int A(\mathbf{r}')W(\mathbf{r}-\mathbf{r}',h)d\mathbf{r}'. \tag{1}$$

If we define a set of points $\mathbf{r}_j$ $(j = 1,2,\ldots,N)$ arbitrarily distributed in the domain, the integral interpolations in Eq. (1) can be approximated by a summation

$$A(\mathbf{r}) \approx \sum_j V_j A_j W(|\mathbf{r}-\mathbf{r}_j|,h), \tag{2}$$

where the index j runs over all the particles present in the influence area (estimated by the length h) centered in $\mathbf{r}$, and $V_j = m_j/\rho_j$ is the volume associated to particle j. Analogously, the derivatives of $A(\mathbf{r})$ can be written as

$$\nabla A(\mathbf{r}) \approx \sum_j V_j A_j \nabla W(|\mathbf{r}-\mathbf{r}_j|,h). \tag{3}$$

A. Equations of motion

The compressible Navier-Stokes equations in a Lagrangian framework can be formulated as

$$\frac{d\mathbf{v}}{dt} = -\frac{\nabla p}{\rho} + \frac{\eta}{\rho}\nabla^2\mathbf{v} + \frac{1}{\rho}\left(\xi + \frac{\eta}{3}\right)\nabla\nabla\cdot\mathbf{v} + \mathbf{F}, \tag{4}$$

where $\mathbf{v}$ and ρ are the fluid velocity and density, respectively, p is the pressure, η and ξ are the dynamic shear and bulk viscosity, and $\mathbf{F}$ is an external body force. A simple equation of state relating pressure to density is, for example,

$$p = \frac{c_s^2\rho_0}{\gamma}\left[\left(\frac{\rho}{\rho_0}\right)^{\gamma} - d\right], \tag{5}$$

where ρ_0 is a reference density, c_s the speed of sound, and γ the ratio of specific heats. Values considered here are $\gamma = 7$ and $d = -1$.

B. Density equation

In SPH the mass density of particle i can be evaluated in conservative fashion as

$$\rho_i = \sum_j m_j W_{ij}, \tag{6}$$

where m_j is the mass associated to particle j and $W_{ij} = W(|\mathbf{r}_i - \mathbf{r}_j|)$ is a suitable kernel function.

C. Momentum equation

The SPH momentum equation (4) evaluated on particle i can be divided into three parts:

$$\frac{d\mathbf{v}_i}{dt} = \left(\frac{d\mathbf{v}_i}{dt}\right)^p + \left(\frac{d\mathbf{v}_i}{dt}\right)^v + \mathbf{F}_i. \tag{7}$$

The SPH discretization of the pressure term can be written as

$$\left(\frac{d\mathbf{v}_i}{dt}\right)^p = -\sum_j m_j\left(\frac{p_i}{\rho_i^2} + \frac{p_j}{\rho_j^2}\right)W'_{ij}\mathbf{e}_{ij}, \tag{8}$$

where $W'_{ij} = \frac{\partial W(r)}{\partial r}|_{r=r_{ij}}$ and $\mathbf{e}_{ij} = \mathbf{r}_{ij}/r_{ij}$. For the discretization of the viscous term, the formulation proposed by Español [14] is chosen, which reads

$$\left(\frac{d\mathbf{v}_i}{dt}\right)^v = -\frac{5}{3}\eta\sum_j m_i\frac{1}{\rho_i\rho_j}[\mathbf{v}_{ij} + \mathbf{e}_{ij}\mathbf{e}_{ij}\cdot\mathbf{v}_{ij}]\frac{W'_{ij}}{r_{ij}}, \tag{9}$$

where the bulk viscosity ξ was set to zero. Notice, however, that, according to Español and Revenga [14] the compressible term $\frac{\eta}{3\rho}\nabla\nabla\cdot\mathbf{v}$ is still included in our model [Eq. (9)], which introduces a dissipation on the dilatational part of the velocity field. Therefore, this formulation is applicable to both incompressible and compressible flows. The external force $\mathbf{F}$ will be discussed in the next section.

III. FORCING SCHEME IN STEADY FORCED TURBULENCE

The forcing scheme adopted in this work to produce a steady homogeneous isotropic turbulent state corresponds to the method proposed by Kida and Orszag [13]. Originally developed for compressible turbulence it can be applied to excite dilatational and solenoidal modes separately. It consists of the following force F applied in real space (domain $[0,L]^3$, with $L = 2\pi$):

$$F_\alpha(\mathbf{x},t) = A_{\alpha\beta}(t)\sin x_\beta + B_{\alpha\beta}(t)\cos x_\beta, \tag{10}$$

where α,β denote Cartesian components, and Einstein summation over repeated indices has been adopted. $\mathbf{A}(t) = A_{\alpha\beta}(t)$ and $\mathbf{B}(t) = B_{\alpha\beta}(t)$ are matrices of Gaussian random variables with zero mean. The elements of $\mathbf{A}(t)$ and $\mathbf{B}(t)$ are mutually statistically independent.

The diagonal and off-diagonal elements are responsible for the forcing of dilatational and solenoidal modes, respectively. For isotropy the following relation must be satisfied:

$$\overline{A_{\alpha\beta}^2} = \overline{B_{\alpha\beta}^2} = \begin{cases} \dfrac{2F_C}{3\Delta t}, & \alpha = \beta \\ \dfrac{F_R}{3\Delta t}, & \alpha \neq \beta \end{cases}. \tag{11}$$

Accordingly, the total energy increases as

$$\epsilon_0 = \frac{d}{dt}\langle E_T\rangle = \langle\rho\rangle(F_C + F_R), \tag{12}$$

where ϵ_0 is the energy injection rate. For stationary turbulence, the energy dissipation rate $\epsilon = \nu\langle|\nabla\mathbf{v}|^2\rangle$ equals ϵ_0, so that the total kinetic energy satisfies $dE_k/dt = \epsilon - \epsilon_0 = 0$.

IV. NUMERICAL RESULTS

We used the standard SPH method to simulate forced compressible turbulence in a periodic cubic box of size ($L = 2\pi$). Two sets of simulations are considered, with a total number of particles $N = N_x \times N_y \times N_z = 32^3$ and $N = N_x \times N_y \times N_z = 64^3$, respectively. Initially all the particles are placed on a cubic lattice with uniform spacing $\Delta x = L/N_x$, and with zero velocities. The Kida-Orszag forcing eventually produces a stationary turbulent motion. In order to eliminate effects of dilatational modes we set $F_C = 0$ and $F_R = 0.01$ in Eq. (11), which gives a dissipation rate $\epsilon = 0.01$, assuming that $\langle\rho\rangle \approx 1$. The input viscosity considered is in the range $\nu \in [10^{-4} - 2 \times 10^{-3}]$, which allows us to define a nominal Reynolds number $150 \leqslant \mathrm{Re} = Lv'/\nu \leqslant 70\,000$, where L is the energy-injection length scale and v' is the root-mean-square velocity. The corresponding nominal Taylor-Reynolds numbers for isotropic and homogeneous turbulence are in the range $40 \leqslant \mathrm{Re}_\lambda \leqslant 1000$. Note that in SPH models using artificial viscosity [11], the minimum employed coefficient is about $\alpha \sim 0.1$, which corresponds to a physical viscosity of $\nu = \frac{\alpha c_s h \rho_0}{10}$. The comparison with equivalent artificial viscosity values corresponding to $\alpha > 0.1$ gives in our case a minimal meaningful viscosity in the range 10^{-5}–10^{-4}.

The smallest turbulent length and time scales that would define the necessary resolution limit of fully resolved direct numerical simulations are on the order of the Kolmogorov length scale $\eta = (\nu^3/\varepsilon)^{1/4}$ and the Kolmogorov time scale $\tau_\eta = (\nu/\varepsilon)^{1/2}$. A speed of sound c_s in Eq. (5) is considered such that the corresponding root-mean-square Mach number is $\mathrm{Ma} = v'/c_s = 0.1, 0.5, 1, 3, 10$. A commonly used kernel function in SPH is the Lucy kernel with overlap $\kappa = 3$, which gives a smoothing length $h = \kappa \Delta x = 3\Delta x$,

$$W(r,h) = w_0 \begin{cases} (1 + 3r/h)(1 - r/h)^3, & r/h < 1 \\ 0, & r/h \geqslant 1 \end{cases}, \tag{13}$$

where w_0 is $105/16\pi h^3$ in three dimensions. Simulations are performed for eight dynamical times $T_D = L/2v'$.

Data are extracted after the initial transient, when the simulation achieves the stationary state. This was monitored through the variation of the kinetic energy E_K. Note that the Kolmogorov scale is much smaller than the initial particle separation Δx; therefore the current setup intentionally considers under-resolved discretizations. Simulations are stable over the entire duration of the run, and we did not observe any blowups. Figure 1 (a) shows the logarithm of the column density field in the xy plane at time $t = 3T_D$ for Ma = 3. Figure 1(b) shows the projection of the divergence of the corresponding velocity field.

A. Energy spectrum

For isotropic turbulence, kinetic-energy spectra exhibit an inertial-range scaling

$$E(k) \propto k^\alpha, \tag{14}$$

where k is a wave number. For incompressible flow $\alpha = -5/3$ is predicted by the Kolmogorov theory. For increasing Mach number the dilatational components of the velocity become more significant, and at highly supersonic flow it is expected, although not shown experimentally, that the kinetic-energy spectrum may be closer to shock-dominated turbulence with $\alpha = -2$ [15].

We have computed the energy spectrum for different time steps and have averaged the results when the flow had achieved a stationary state. The nominal Reynolds number was $\mathrm{Re}_\lambda = 983$ for a Mach number Ma = 10. This setup corresponds to the choice of a Kolmogorov wave number $k_\eta = \pi/\eta \approx 980 \gg k_{\max} = 16$ for an SPH-particle number $N = 32^3$.

The energy spectrum is calculated as follows: The velocity field has first been interpolated onto a grid. For each velocity component, Fourier transforms of the velocity field $\mathbf{v} = (v_x, v_y, v_z)$ [denoted as $\mathbf{V} = (V_{k_x}, V_{k_y}, V_{k_z})$] have been computed. Using these definitions the velocity spectrum tensor is evaluated as

$$E(\mathbf{k}) = \tfrac{1}{2}\,|\mathbf{V}(\mathbf{k}) \cdot \mathbf{V}^*(\mathbf{k})|\,, \tag{15}$$

where $\mathbf{V}^*$ is the complex conjugate of the transformed velocity. $\mathbf{k} = (k_x, k_y, k_z)$ is the wave number. The energy spectrum $E(k)$ is finally obtained as $E(k) = 4\pi k^2 \langle E(\mathbf{k})\rangle$, where $\langle \cdots \rangle$ denotes an average over the thin spheric shells of radius $k = |\mathbf{k}|$.

Figure 2(a) shows the evolution of the instantaneous energy spectrum from the initial state to the stationary state. The dashed (blue) lines correspond to spectra evaluated at different snapshots during the transient, and the dash-dot lines (red and light blue) indicate that a self-similar spectrum evolves gradually. In order to extract the slope, we have averaged 70 snapshots of the energy spectrum at the steady state, between $t = 2T_D - 8T_D$ every $\Delta T = 0.1 T_D$, as shown in Fig. 2(b). The slope obtained in our simulation is $\alpha = -1.9$, which is in good agreement with previous results reported in Refs. [11,16], where $\alpha \in [-1.87, -1.95]$. Note that the energy spectrum deviates slightly from the power scaling for wave numbers $k > 10$. The deviation may either be due to numerical dissipation at large wave numbers due to the SPH discretization scheme, or it may be due to interpolation of particle data from random locations back to a grid for postprocessing for which high-order M_4' moments-preserving kernel [17] were used. Note that there are currently no techniques which allow us to perform an accurate estimate of the energy spectrum from Lagrangian velocity field up to the maximum wave number $k_{\max} = N/2$, e.g., in Ref. [18] the use of discrete Fourier transform allows to obtain an accurate spectrum up to $k = 0.26N$, substantially smaller than $k_{\max}$ [18]. This represents a potential drawback for the evaluation of turbulence models in SPH which needs to be addressed in the future.

B. Density PDF

The PDF of the density is important for characterizing supersonic turbulence. Previous studies [19–21] have shown that the density PDF of flows is well represented by a lognormal distribution

$$p(\rho) = \frac{1}{\sqrt{2\pi\sigma^2}} \exp\left[-\frac{1}{2}\left(\frac{\ln\rho - \overline{\ln\rho}}{\sigma}\right)^2\right], \tag{16}$$

where the standard deviation σ and the mean $\overline{\ln\rho}$ are functions of the fluctuating Mach number (i.e., the root mean square of

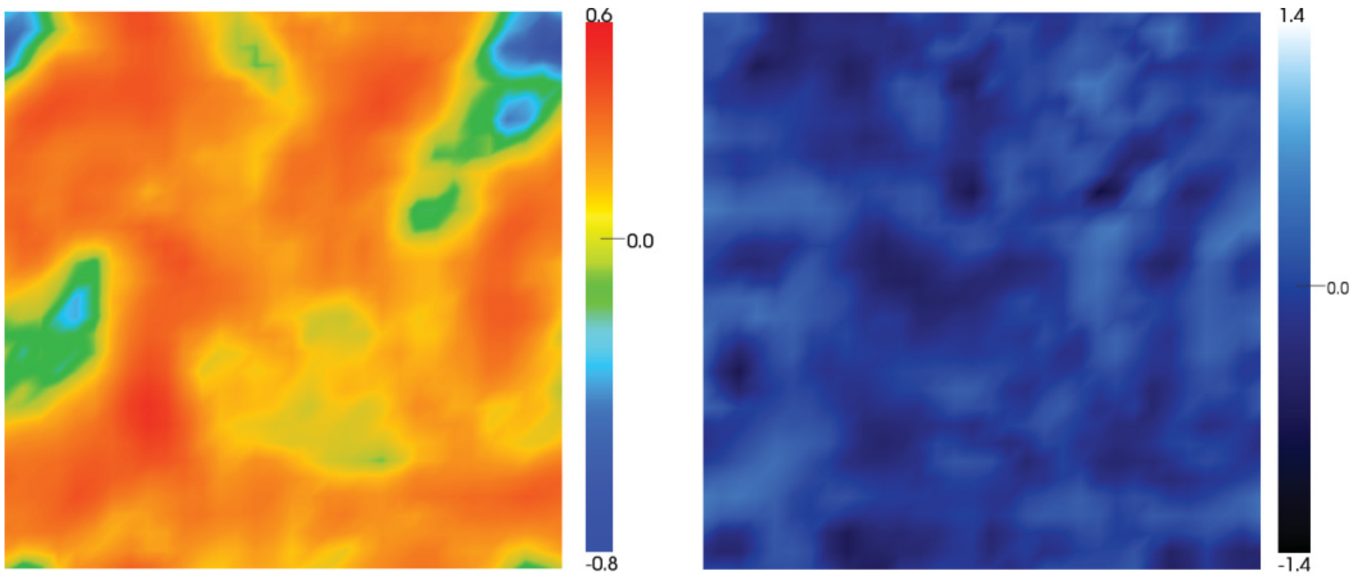

(a) projected column density in log (b) projected divergence $\nabla \cdot v$ (10^1)

FIG. 1. (Color online) (a) column density from a snapshot at time $t = 3T_D$ for Ma $= 3$. (b) Projected divergence of the velocity field $\nabla \cdot v$. Negative (positive) values correspond to regions of local compression (rarefaction), respectively.

the local Mach number) M':

$$\overline{\ln \rho} = -\frac{\sigma^2}{2} \tag{17}$$

and

$$\sigma^2 = \ln(1 + b^2 M'^2). \tag{18}$$

Figure 3 presents the time-averaged density PDF $p(\rho)$ obtained for solenoidal random forcing and two particle numbers $N = 32^3$ and 64^3. The PDF in the inset of Fig. 3 shows clearly a lognormal distribution in agreement with previous calculations and with theoretical expectations, except for very small probabilities (see the main plot of Fig. 3), where our simulation indicates deviations from the lognormal distribution. Federrath and coauthors also found a deviation from the lognormal distribution near the PDF tails [16]. The deviations were explained by rare events caused by strongly intermittent fluctuations during head-on collisions of strong shocks and oscillations. Shock-induced intermittency should be therefore the basis of non-Gaussianity in the density PDF and can be quantified by the onset of a weak correlation between density and velocity fields as discussed in Ref. [20].

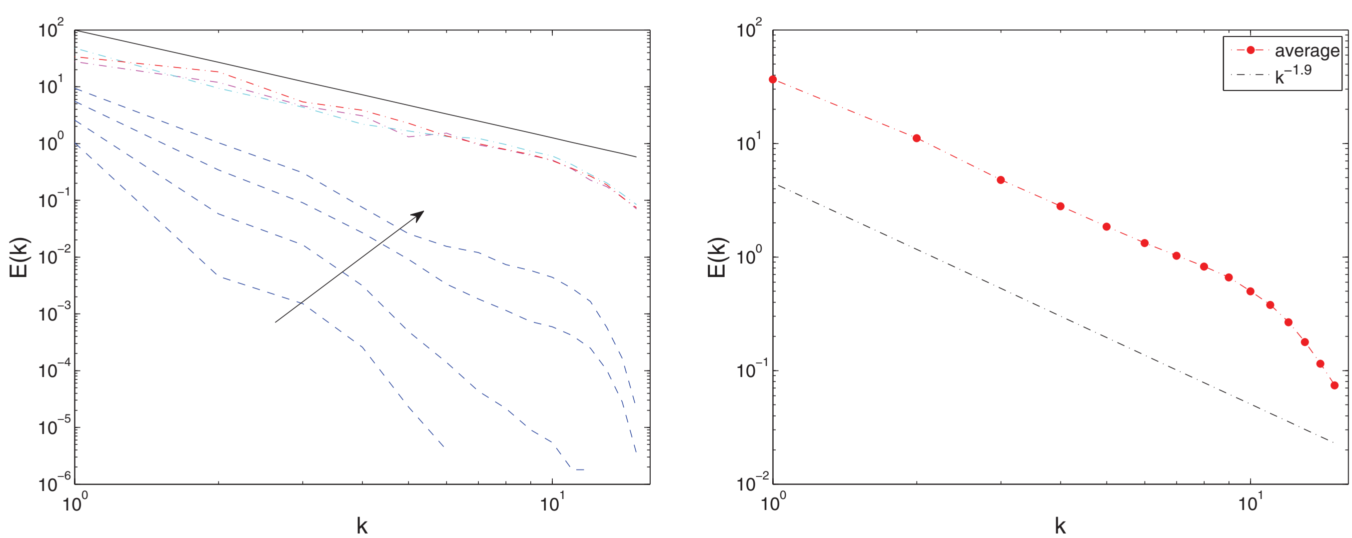

(a) Temporal evolution of energy spectrum (b) Averaged energy spectrum at stationary state

FIG. 2. (Color online) Energy spectrum at Ma $= 10$. (a) Time evolution of the energy spectra (dashed blue line) evaluated at different snapshots during the transient. The blue and red dashed-dot lines indicate the self-similar spectrum. (b) Averaged energy spectrum at steady state.

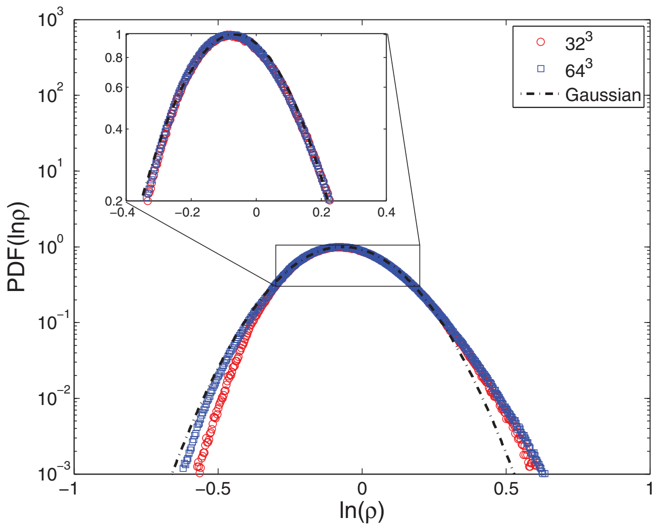

FIG. 3. (Color online) PDF of $\ln\rho$ at $\mathrm{Ma} = 3$ with resolutions of 32^3 and 64^3 and $\mathrm{Re}_\lambda = 943$. The inset shows clearly a lognormal distribution for large probabilities of the density PDF. Deviations from the lognormality appear at smaller probabilities.

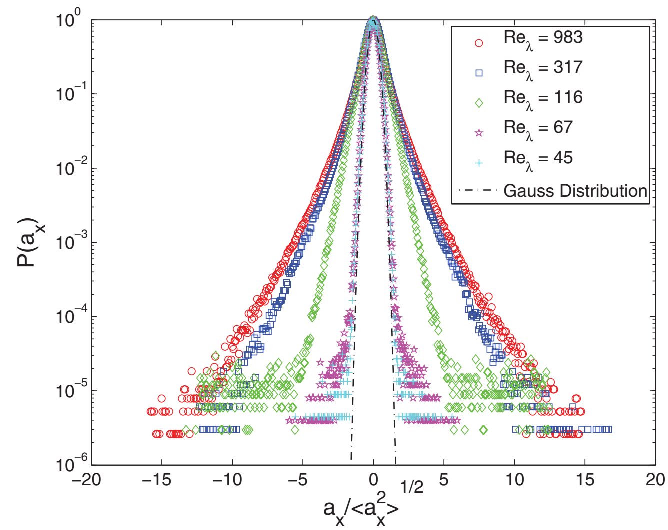

FIG. 4. (Color online) PDF of acceleration for different Reynolds numbers.

It should be noted that, although exhibiting intermittency, the maximum density fluctuations in our simulation are not as large as those reported in Refs. [11,16], and the best-fitting lognormal distribution gives $b \approx 0.14$, which is smaller than 0.33 as in Ref. [22]. In order to check the reason for this discrepancy, we have performed a systematic study to investigate the effect of several SPH model parameters. We have insignificant changes of the results when different parameters γ and d in the equation of state were used (values $\gamma = 1,7$ and $d = 0,-1$ were tested) provided that the effective speed of sound was kept constant. The same holds also for the PDF of acceleration and scaling exponent, discussed in the following sections. Furthermore, one can see from Fig. 3 that an increased particle resolution only slightly affects the density PDF and thus cannot explain the differences from Ref. [11]. Although different particle resolutions affect the tails of the density PDF, low-order moments of the PDF are hardly affected: We have evaluated the skewness of the PDF in Fig. 3 for $N = 32^3, 64^3$ giving, respectively, $s_1 = 0.833$ and $s_2 = 0.838$, and the relative error of skewness for two resolutions is consistently less than 1%. For the Reynolds number in the range $\mathrm{Re}_\lambda \in [200 - 1000]$, there are only very slight differences of density PDF among various Re_λ. In conclusion, we identify the real-space forcing scheme used here as the only possible main cause of the discrepancy with respect to the results reported in Ref. [11] where a spectral forcing scheme was adopted. Some evidence supporting this view can be found for example in Ref. [23]. In this work the authors obtain $b = 0.26$, even though the forcing was not purely solenoidal, suggesting that for a pure solenoidal forcing, an even smaller b value could be expected. Also, the strong influence of the forcing scheme on the density PDF has been already reported in Ref. [16] and should be carefully taken into account when aiming at quantitative comparisons.

C. Acceleration PDF

The PDF of particle accelerations is very important for the development of phenomenological and stochastic models of turbulent mixing. With previously employed forcing scheme problems can arise when studying the acceleration PDF of SPH particles. Due to the fact that the forcing scheme introduces a Gaussian acceleration, it is difficult to observe typical non-Gaussian "stretched tails" that are found in experiments [24] and DNS [25]. In order to avoid the effect of the Gaussian distributed external force, we remove the background Gaussian accelerations from the total acceleration acting on the particles; that is, we consider statistics of $\mathbf{a}'_j(t) = \mathbf{a}_j(t) - \mathbf{F}_j(t)$ where $\mathbf{F}_j(t)$ is the stochastic forcing term at time t acting on the particle j.

First, we consider results with the largest Mach number in our simulation, Fig. 4 shows the PDF of accelerations for different Reynolds numbers at $\mathrm{Ma} = 10$. For moderate Reynolds numbers, $45 \leqslant \mathrm{Re}_\lambda \leqslant 300$, the tails of the acceleration PDF extend dramatically, whereas at larger Re_λ they seem to tend toward a limit curve. In order to quantify the degree of intermittency of the accelerations, we calculate the flatness $(\langle a^4\rangle/\langle a^2\rangle^2)$ of their distributions as a function of the Reynolds number.

The slow statistical convergence of the flatness can be remedied by fitting first the scattered data with an analytical function $P(a) = C\exp\{-a^2/[(1 + |a\beta/\sigma|^\gamma]\sigma^2)\}$ as used in Ref. [24] and then evaluating the corresponding flatness.

As a cross-check, we have also computed the flatness directly from the scattered data and indicate error bars in the respective figures. Figure 5(a) shows that the flatness of the acceleration PDF increases significantly in the small Reynolds number range, tending to a finite value at large Reynolds numbers. These results show a similar trend as the measured flatness reported for incompressible turbulence [26]. Note that approaching a limiting curve for increasing Re_λ is not a numerical artifact due to under-resolution. In Fig. 6 the acceleration PDF evaluated from two simulations with particle resolution $N = 32^3, 64^3$ is shown. Good collapse of

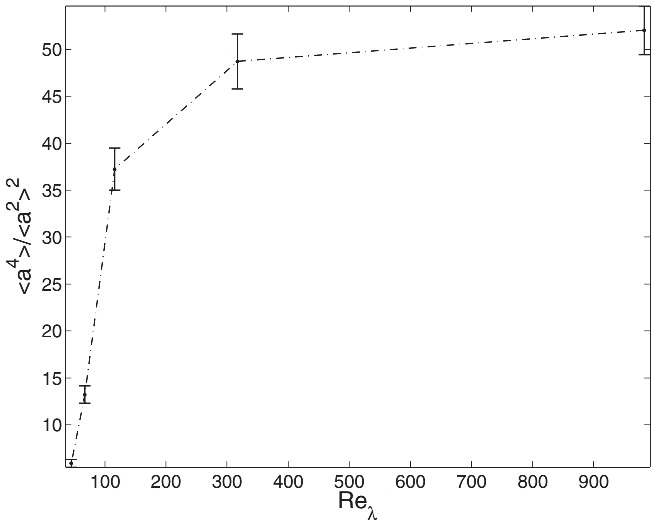

(a) Flatness with different Reynolds number

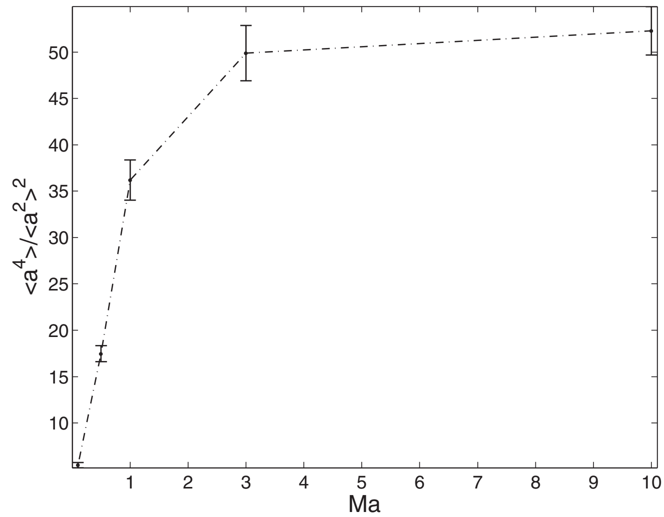

(b) Flatness with different Mach number

FIG. 5. Flatness of the acceleration PDF: Reynolds- and Mach-number dependence. (a) Flatness with different Reynolds number at Ma = 10. (b) Flatness with different Mach number, the maximal Reynolds number has been chosen at each Mach number, such that $\mathrm{Re}_\lambda = 932$, $\mathrm{Re}_\lambda = 946$, $\mathrm{Re}_\lambda = 978$, $\mathrm{Re}_\lambda = 940$, $\mathrm{Re}_\lambda = 983$ for Ma = 0.1, 0.5, 1.0, 3.0, 10, respectively.

the results is obtained up to acceleration events corresponding to dimensionless $|\tilde{a}| \approx 10$, showing that the main intermittent behavior is correctly captured. For very large values of the acceleration, the two curves depart slightly; they correspond, however, to very rare events which do not contribute much to the fourth-order moment of the PDF. We have explicitly checked that the relative difference in flatness between the two curves in Fig. 6 was below 5% indicating that the particle resolutions adopted were large enough to extract the statistics considered here. In particular, $N = 32^3$ and 64^3 give $f_1 = 47.327$ and $f_2 = 49.284$, respectively.

The effects of Mach number on the acceleration PDF have been rarely considered in the literature. Figure 7 shows the acceleration PDF for $\mathrm{Ma} = 0.1, 0.5, 1, 3$ at $N = 32^3$. For small Mach number Ma = 0.1, the PDF exhibits slight

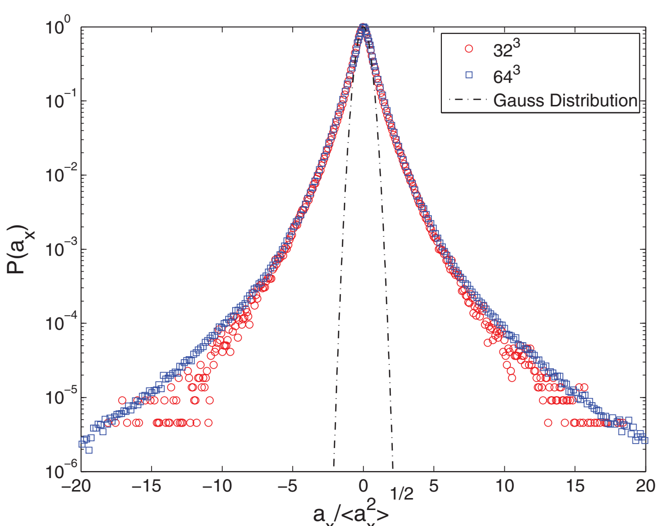

FIG. 6. (Color online) Flatness of PDF of acceleration.

deviations from the Gaussian distribution. With increasing Mach number the PDF becomes much more intermittent. This trend levels off at large Mach numbers; see Fig. 5(b). Unlike for incompressible flow, intermittency in compressible turbulence can by caused by shocks and rarefaction waves, as discussed in Ref. [16]. We have checked the effect of SPH-model parameters, and have found no significant changes of the PDF except for very rare events at the PDF tails.

D. Lagrangian scaling exponents

Scaling exponents, defined as the logarithmic derivative of the Lagrangian structure functions of the respective order, also serve to analyzed intermittency

$$\zeta_p(\tau) = \frac{d\log[S_p(\tau)]}{d\log[S_2(\tau)]}. \tag{19}$$

Here

$$S_p(\tau) = \langle [v(t+\tau) - v(t)]^p \rangle \tag{20}$$

is the Lagrangian structure function of order p and τ is the time lag. $\zeta_p(\tau)$ is a local scaling exponent, and its variation with τ indicates *anomalous scaling*, a typical manifestation of intermittency.

Figure 8 shows the local scaling exponent for different Mach numbers as a function of τ normalized by the Kolmogorov scale, τ/τ_η. A nonintermittent behavior would correspond to a constant value $\zeta_p(\tau) = p/2$. In the range of τ where the scaling exponents $\zeta_p(\tau)$ differ from this value, the velocity field is temporally intermittent. From Fig. 8 it is evident that there is a tendency toward the nonintermittent case $\zeta_4(\tau) = 2$ only for very small time lags $\tau \ll \tau_\eta$ for all the Mach numbers considered. The strongest deviation from the nonintermittent value is observed in the range $\tau_\eta \leqslant \tau \leqslant 5\tau_\eta$, where a minimum in $\zeta_4(\tau)$ is visible. Again, the dip behavior is qualitatively similar to that reported

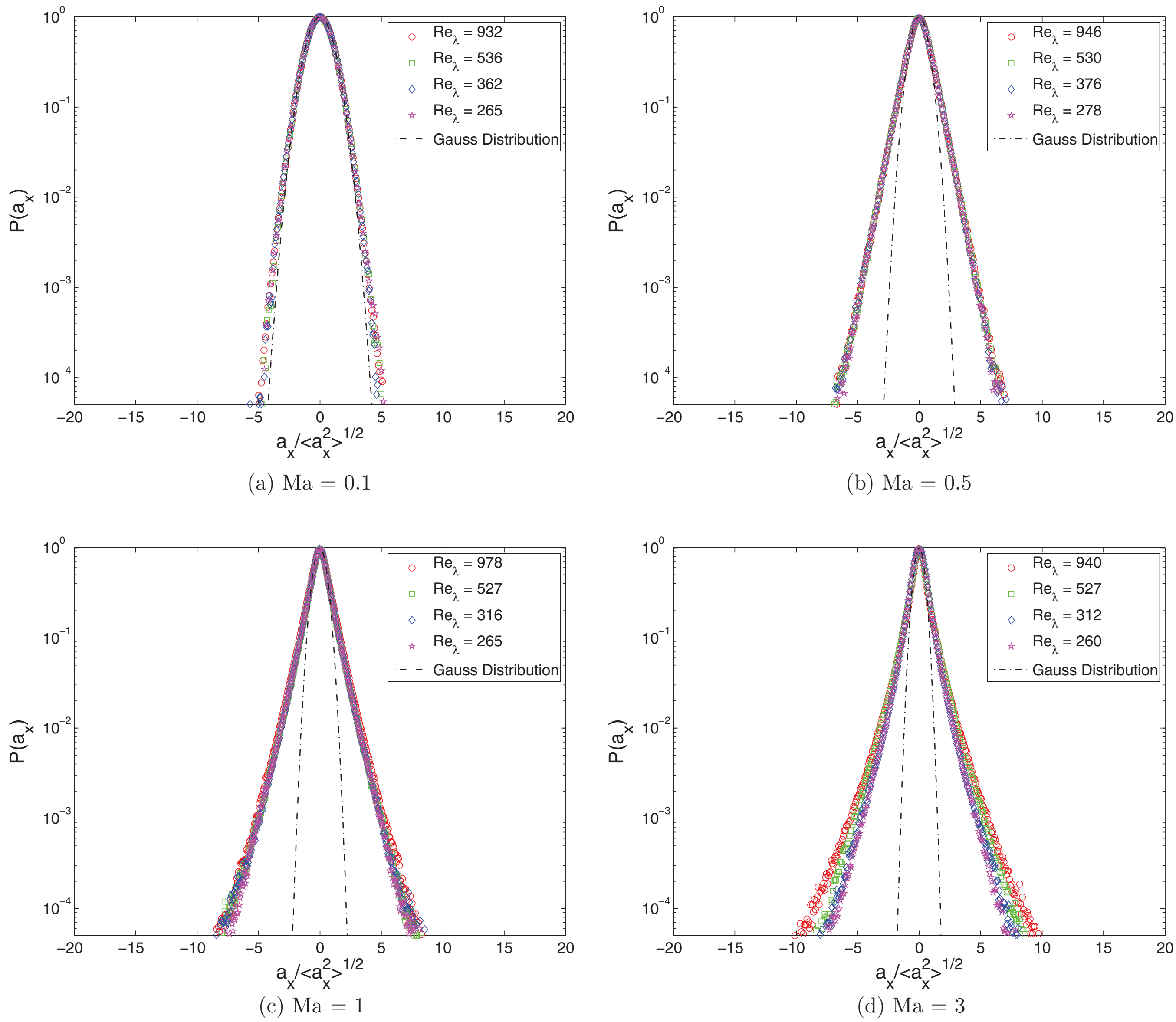

(a) Ma = 0.1 (b) Ma = 0.5 (c) Ma = 1 (d) Ma = 3

FIG. 7. (Color online) PDF of acceleration for different Mach numbers.

for incompressible turbulence in Ref. [7], where, however, intermittency is rather caused by coherent structures of intense vorticity. Such structures intentionally are not resolved by the present SPH simulations, so that they cannot be the reason for the observed intermittency in our case. Evidence of strong correlation between vortical structures and high acceleration events in the incompressible case was reported, for example, in Ref. [27]. The intermittent behavior observed here has a different origin, being caused by strong compression (rarefaction) waves ($\nabla \cdot \mathbf{v}$) of the type discussed, for example, in Ref. [28]. It can be seen that with increasing Mach number intermittency becomes increasingly significant, as the acceleration PDF changes its shape with Mach number in Fig. 7. Larger time lags $\tau \geqslant 5\tau_\eta$ cannot be resolved numerically by the current setup. Note that the resolutions used here are insufficiently to obtain statistically fully converged result [11], which has to be taken into account when assessing the results.

V. CONCLUSIONS

The observation of typical stretched tails in the probability distribution function of particle accelerations made in previous two-dimensional simulations under constant shear flow [12] motivated the research reported here. By discretizing the continuum equations following the motion of fluid particles the SPH method allows us to extract easily Lagrangian statistics, such as multitime correlations and Lagrangian scaling exponents, without the need to introduce extra tracer particles on a precalculated Eulerian velocity fields. When performing under-resolved simulations, the typical cutoff in the Fourier space is at much smaller wave numbers than those for the smallest physical scales characterized by the Kolmogorov length. For creating a stationary statistically isotropic flow field the stochastic forcing scheme proposed by Kida *et al*. [13] is applied. The stationary energy spectrum produces a Burgers-like scaling behavior with an exponent

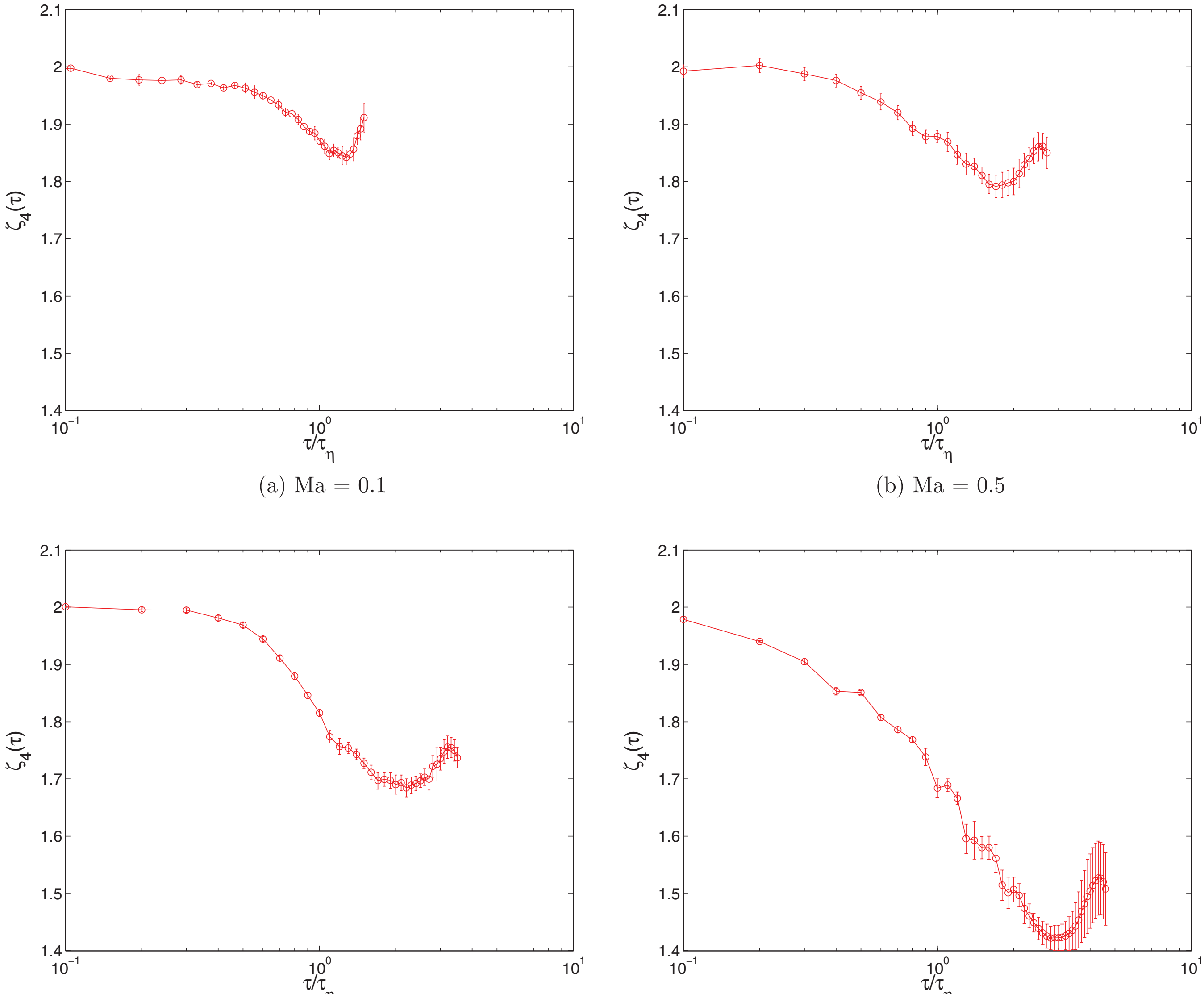

(a) Ma = 0.1 (b) Ma = 0.5 (c) Ma = 1 (d) Ma = 3

FIG. 8. (Color online) scaling exponent.

$\alpha \approx 1.9$ for most of the resolved wave-number range ($k = 10$ for $N = 32^3$) without introducing an explicit turbulent model. At larger k exponential decay is observed. It is, however, difficult to say whether this behavior is the result of an implicit dissipation contained in the SPH method or whether it originates from the particle-grid interpolation used to for evaluating the energy spectra. A lognormal distribution is obtained for most of the density PDF. Deviations from lognormality are observed at the PDF tails, which differ, however, quantitatively from previously reported results. This difference can be attributed to the different forcing scheme used here.

Concerning the PDF of the particle accelerations, we have observed a tendency toward intermittency when increasing Reynolds and Mach numbers. In both cases the flatness of the PDF increases dramatically for low to moderate values of Re and Ma and eventually levels off. Sensitivity tests on the evaluated PDF flatness to SPH resolution have been performed showing no significant effect on the results and indicate that low-order statistics are statistically converged. Intermittent behavior has been analyzed also for Lagrangian structure functions and relative scaling exponents. Anomalous scaling is observed corresponding to departures of ζ_4 from the nonintermittent value 2. Moreover, the slope of $\zeta_4(\tau)$ shows a qualitative behavior that agrees with incompressible results [7]. The magnitude of the $\zeta_4(\tau)$ minimum decreasing with increasing Mach number. It is important to note that the increasing intermittency here is generated by shocklets in the density and pressure fields rather than by coherent vortical structures mentioned in Ref. [7]. Further tests for decaying turbulence as well as for wall-bounded shear flow will be performed in the future in order to study the behavior of compressible intermittency under anisotropic conditions.

ACKNOWLEDGMENTS

We thank D. Price for the useful discussion and for providing us with the spectral forcing scheme. Financial support provided by the DFG via the Grant EL503/1-1 is gratefully acknowledged. Yilei Shi gratefully acknowledges the support of the TUM-Graduate School's Faculty Graduate Center Mechanical Engineering at the Technische Universität München.

[1] G. Gulitski, M. Kholmyansky, W. Kinzelbach, B. Luethi, A. Tsinober, and S. Yorish, J. Fluid Mech. **589**, 57 (2007).
[2] T. Ishihara, Y. Kaneda, M. Yokokawa, K. Itakura, and A. Uno, J. Fluid Mech. **592**, 335 (2007).
[3] N. Mordant, E. Leveque, and J. Pinton, New J. Phys. **6**, 116 (2004).
[4] N. M. Qureshi, M. Bourgoin, C. Baudet, A. Cartellier, and Y. Gagne, Phy. Rev. Lett. **99**, 184502 (2007).
[5] M. Bourgoin, N. Ouellette, H. Xu, J. Berg, and E. Bodenschatz, Science **311**, 835 (2006).
[6] R. Volk, N. Mordant, G. Verhille, and J. Pinton, Europhys. Lett. **81**, 34002 (2008).
[7] F. Toschi and E. Bodenschatz, Annu. Rev. Fluid Mech. **41**, 375 (2009).
[8] L. Lucy, Astron. J. **82**, 1013 (1977).
[9] R. A. Gingold and J. J. Monaghan, Mon. Not. R. Astron. Soc **181**, 375 (1977).
[10] J. J. Monaghan, Rep. Prog. Phys. **68**, 1703 (2005).
[11] D. Price and C. Federrath, Mon. Not. R. Astron. Soc **406**, 1659 (2010).
[12] M. Ellero, P. Español, and N. A. Adams, Phy. Rev. E **82**, 046702 (2010).
[13] S. Kida and S. Orszag, J. Sci. Comp. **5**, 85 (1990).
[14] P. Espanol and M. Revenga, Phy. Rev. E **67**, 026705 (2003).
[15] E. Falgarone and T. Passot, *Turbulence and Magnetic Fields in Astrophysics* (Springer Verlag, Heidelberg, Germany, 2003).
[16] C. Federrath, J. Duval, R. Klessen, W. Schmidt, M. Mac Low, Astron. Astrophys. **512**, A18 (2010).
[17] G. Cottet and P. Koumoutsakos, *Vortex Methods: Theory and Practice* (Cambridge University Press, Cambridge, UK, 2000).
[18] M. Robinson and J. J. Monaghan, Int. J. Numer. Meth. Fluids (2011), doi:10.1002/fld.2677.
[19] P. Padoan, A. Nordlund, and B. J. T. Jones, Mon. Not. R. Astron. Soc **288**, 145 (1997).
[20] T. Passot and E. Vazquez-Semadeni, Phys. Rev. E **58**, 4501 (1998).
[21] R. S. Klessen, Astrophys. J. **535**, 869 (2000).
[22] D. Price, C. Federrath, and C. M. Brunt, Astrophys. J. Lett. **727**, L21 (2011).
[23] A. G. Kritsuk, M. L. Norman, P. Padoan, and R. Wagner, Astrophys. J. **665**, 416 (2007).
[24] A. La Porta, G. Voth, A. Crawford, J. Alexander, and E. Bodenschatz, Nature (London) **409**, 1017 (2001).
[25] L. Biferale, G. Boffetta, A. Celani, B. J. Devenish, A. Lanotte, and F. Toschi, Phys. Rev. Lett. **93**, 64502 (2004).
[26] G. A. Voth, A. la Porta, A. M. Crawford, J. Alexander, and E. Bodenschatz, J. Fluid Mech. **469**, 121 (2002).
[27] S. Lee and C. Lee, Phys. Rev. E **71**, 056310 (2005).
[28] R. Samtaney, D. I. Pullin, and B. Kosovic, Phys. Fluids **13**, 1415 (2001).